Membrane Assembly in Retinal Photoreceptors

I. Freeze-fracture Analysis of Cytoplasmic

Vesicles in Relationship to Disc Assembly

JOSEPH C. BESHARSE and KARL H. PFENNINGER

Department of Anatomy, Emory University School of Medicine, Atlanta, Georgia 30322, and
Department of Anatomy, College of Physicians and Surgeons, Columbia University, New York 10032

ABSTRACT   To study precursor-product relationships between cytoplasmic membranes of the inner segment of photoreceptors and the continually renewed outer disc membrane, we have compared the density and size distribution of intramembrane particles (IMP) in various membrane compartments of freeze-fractured photoreceptor inner and outer segments. Both rod and cone outer segments of *Xenopus laevis* are characterized by a relatively uniform distribution of ~4,400–4,700 IMP/μm^2 in P-face (PF) leaflets of disc membranes. A similar distribution of IMP is found in the outer segment plasma membrane, the ciliary plasma membrane, and in the plasma membrane of the inner segment in the immediate periciliary region. In each case the size distribution of IMP can be characterized as unimodal with a mean diameter of ~10 nm. PF leaflets of endoplasmic reticulum, Golgi complex, and vesicles near the cilium have IMP with a size distribution like that in the cilium and outer segment, but with an average density of ~2,000/μm^2. In contrast, IMP are smaller in average size (~7.5 nm) in PF leaflets of inner segment plasma membrane, exclusive of the periciliary region. The similarity of size distribution of IMP in inner segment cytoplasmic membranes and those within the plasmalemma of the cilium and outer segment suggest a precursor-product relationship between the two systems. The structure of the vesicle-rich periciliary region and the segregation of IMP with different size distributions in this region suggest that components destined for incorporation into the outer segment exist as preformed membrane packages (vesicles) which fuse with the inner segment plasma membrane in the periciliary region. Subsequently, membrane components may be transferred to forming discs of the outer segment via the ciliary plasma membrane.

Vertebrate photoreceptors are composed of a photosensitive outer segment (ROS), an inner segment that contains the cell's metabolic machinery (i.e., endoplasmic reticulum, Golgi complex, ribosomes, mitochondria), and a synaptic terminal at which contacts with second-order neurons of the retina are made. The photosensitive outer segment (Fig. 1) is connected to the inner segment by a modified, nonmotile cilium (42), and consists of a series of discrete membranous discs that are apparently derived from the plasma membrane in the region of the connecting cilium (32). The process of disc assembly, which continues throughout the life of the cell (49, 50), is widely believed to involve infolding of ROS plasma membrane (32) or protrusion of ciliary plasma membrane (1). Either

mechanism, however, requires a means for plasma membrane expansion. For example, in rod photoreceptors of *Xenopus laevis* ~64 new discs, corresponding to ~3,600 μm^2 of membrane per rod, are formed during the first 8 h of light each day (5, 6). In the photoreceptors in which those measurements were made, however, the combined surface areas of the ROS plasma membrane and cilium was only ~500 μm^2 (4, 7). Thus, a mechanism for expansion of the plasma membrane must exist if discs are derived from it.

A potential mechanism is that membrane precursor is delivered to the ciliary region as preformed membrane packages which are then incorporated into the plasma membrane (4, 24, 35). Once incorporated into plasma membrane those compo-
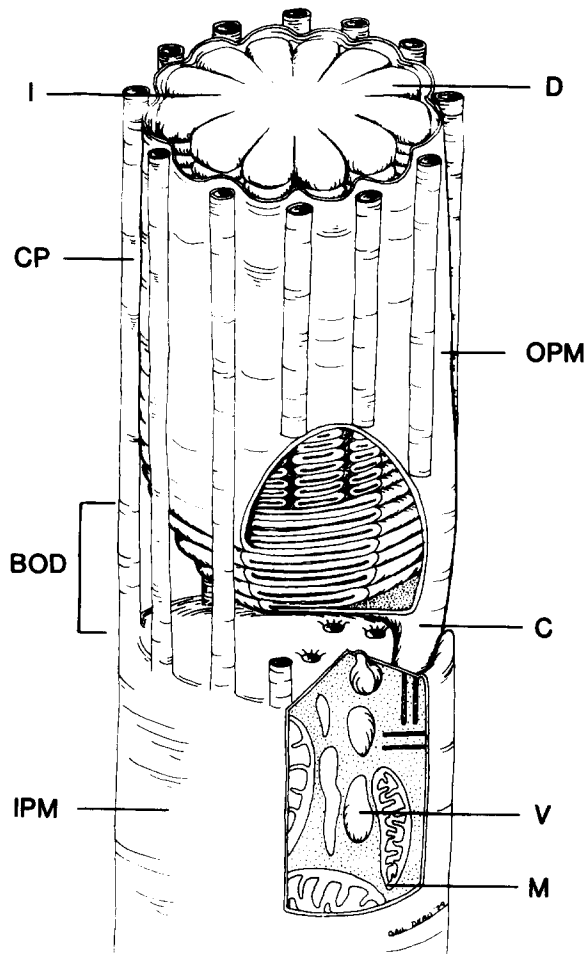
FIGURE 1 Diagrammatic representation of the inner segment-outer segment junction of an amphibian rod photoreceptor based on ultrastructural data. The outer segment is surrounded by calycal processes (*CP*, microvillous extensions of the inner segment), but the only site of cytoplasmic and membrane continuity is at the cilium (*C*). The plasmalemma of the cilium is confluent distally with the outer segment plasma membrane (*OPM*) and zone of basal open discs (*BOD*); proximally it is confluent with the inner segment plasmalemma (*IPM*). In cutaway view, mitochondria (*M*) and membrane vesicles (*V*), consistent features of the periciliary region, are illustrated. Sites of continuity of vesicles with the plasma membrane are illustrated adjacent to the cilium. Additional abbreviations: *D*, outer segment disc; *I*, disc incisure.

nents destined for the outer segment could move via the plasmalemma of the cilium into forming discs or outer segment plasma membrane. This hypothesis is in part analogous to that of secretion in pancreatic exocrine cells and that of axolemmal expansion in neurons (20, 34, 40, and footnote 1) and is consistent with the observation that opsin, the apoprotein of visual pigment, destined for the outer segment may be isolated in association with sedimentable membrane vesicles (also called "schleppersomes"; 35, 36). Although membrane vesicles and cisternae have been described in the region immediately adjacent to the cilium of both embryonic and mature photoreceptors (Fig. 1; see also references 4, 21, and 24), a major unan-

---

[1] Pfenninger, K. H., and M.-F. Maylié-Pfenninger. 1980. Relative movement and appearance of lectin receptors during plasmalemmal expansion in the neuron. Manuscript submitted for publication.

swered question is whether or not such vesicles are involved in disc assembly?

In an attempt to answer this question, we recently initiated a series of morphological studies involving freeze-fracture, horseradish peroxidase uptake, immunocytochemistry, and electron microscope autoradiography on cytoplasmic vesicles in photoreceptors during periods of rapid membrane assembly evoked by exposure to light. The present paper describes the results of a freeze-fracture analysis of both rod and cone photoreceptors of *X. laevis*. The rationale was to compare the size distributions and densities of IMP of different membranes along the vectorial pathway of outer segment assembly. The results are consistent with the idea that periciliary vesicles are involved in the process of membrane expansion.

MATERIALS AND METHODS

Animals and Experimental Treatment

X. laevis tadpoles (31; stages 56–57) and adults (~8–10 cm) were maintained in cyclic light (12L:12D) at room temperature (22°–25°C). Tadpoles were fed parboiled spinach and adults were fed commercial food pellets (Nasco, Inc., Fort Atkinson, Wis.) or chopped beef liver. Although rod photoreceptor length increases during the postmetamorphic period, we have not found differences related to developmental stage among the features analyzed in the present report. Animals prepared for general microscopy and freeze-fracture were killed at 0, 2, 4, 6, and 8 h after the normal onset of light; a period during which disc assembly is maximized (6).

Microscopy

For thin sectioning, eyes were fixed by immersion in a mixture of 2% paraformaldehyde, 2.5% glutaraldehyde, and either 0.067 or 0.1 M cacodylate buffer at pH 7.4. After removal of eyes, an incision was made through the cornea to allow penetration of the fixative, and after fixation, the cornea, lens, and iris were removed. Eye cups were washed for 10–20 min in 0.1 M cacodylate buffer containing 0.2 M sucrose and postfixed for 1 h in 1% OsO$_4$ in the same buffer before dehydration with ethanol and propylene oxide and embedment in an Epon-Araldite mixture.

For freeze-fracture, eyes were fixed 4 h in the fixative containing 0.1 M buffer and were washed overnight using three changes of the buffer-sucrose solution. The washing medium was then gradually replaced over a period of 45 min with 25% glycerol in 0.1 M cacodylate buffer. Eye cups were then immediately transferred to specimen holders (two to three eye cups/holder) and frozen by rapid immersion in Freon 22 maintained near liquid nitrogen temperature. Retinas were stored in liquid nitrogen until fracturing in a Balzer's freeze-fracture unit equipped with a quartz crystal thin film monitor. Retinas were fractured at −115°C under a vacuum of <10^{-6}mbar and etched for 30 s before evaporation of platinum-carbon from an electron beam gun. During etching the specimen surface was shielded with the knife holder. Replicated tissues were then transferred to 2.0 M NaCl which was gradually replaced with Chlorox to dissolve the tissue. After several hours of Chlorox treatment, replicas were washed in distilled water, collected on 200-mesh Formvar-coated grids, and examined with a Phillips 400 electron microscope.

Analysis of Replicas

Quantitative data were obtained from some 30 replicas, each formed over the fractured surface of two to three retinas. IMP densities in flat areas of each membrane system were determined from electron micrographs at × 100,000. Large expanses of fractured discs and plasma membrane were exposed in most replicas and the total areas sampled were substantial (2–5 μm^2). Other membrane systems, particularly ciliary plasma membrane, were rare in replicas and, as a consequence, the total sampled area was <1 μm^2 in each case. To sample rare membrane components, counts were obtained from multiple small areas (0.01 μm^2) until representative regions of the particular membrane were no longer available. Generally 25 or more counts were obtained, but, in the case of ciliary plasma membrane, only eight such areas were analyzed for IMP density and size distribution.

The only exception to the above procedure was for the cytoplasmic vesicles of the periciliary and Golgi regions. Because vesicles most often approximated either a sphere or ellipsoid, we corrected for potential underestimation of surface area by two methods. First, we selected vesicles with a shadow filling about one-half the interior of the vesicles, and counted and measured IMP visible in the

unshadowed half. Such profiles were regarded as hemispheres or hemiellipsoids, a conclusion justified by the geometry of replica formation for spherical vesicles (47); the area to which the IMP counts were referenced was one quarter the surface area of a sphere or ellipsoid having the dimensions measured for the profile. In the second approach we selected vesicle profiles which lacked a shadow and were assumed to have a near-planar area. In theory this approach overestimates the IMP density by not taking into account the slight membrane curvature, but in practice the error is small relative to that involved in IMP counting (47). A variant of this approach was used for convex (E-face [EF] leaflet) profiles in which IMP were tabulated in areas that were small relative to size of the profile. However, because so few IMP were seen in convex profiles, the values presented in this paper for EF leaflets of the Golgi complex and vesicles (Table I) are only a gross estimate.

We also estimated sizes of IMP in each membrane system by measuring the greatest width of the shadow in a plane perpendicular to the direction of shadowing. IMP were measured with a dial caliper at a final magnification of 275,000. These data were used to generate size-frequency histograms and average IMP sizes for comparison of the various membrane regions (Fig. 8). Sample size of measured IMP ranged from 71 to 258 for PF leaflets and from 26–96 for EF leaflets. Data on both density and IMP size were analyzed statistically using analysis of variance, and where appropriate differences between individual pairs of means were tested for statistical significance using Duncan's New Multiple Range Test (15).

RESULTS

Membranes of the Inner Segment

In both rods and cones of *X. laevis* the periciliary region consistently exhibits a variety of irregular, smooth vesicles and cisternae and an irregular, ruffled configuration of the adjacent inner segment plasma membrane (Fig. 2–4). The configuration of the plasma membrane is that of a series of deep depressions (Fig. 4). Close association of smooth vesicles with the depressions in most sections through the periciliary region suggests that the cell is actively engaged in either endocytosis or exocytosis. In this same region the cell surface has a well-developed fuzzy surface that extends over the openings of depressions to form a diffuse covering (Fig. 4). In addition to the clear vesicles in the periciliary region, we have also detected a prominent population of "cup-like" vesicles (Fig. 2), and have also seen cisternae of rough endoplasmic reticulum (RER) as well as smooth endoplasmic reticulum (SER). The latter two membrane systems appear to be extensions of endoplasmic reticulum more prominently developed in the myoid. The SER is similar in structure to that implicated in synaptic vesicle turnover in *Rana pipiens* photoreceptors (21, 43), and has been suggested to play a role in ROS disc renewal (30).

Because of the large population of mitochondria, the adjacent ROS, plasmalemmal depressions, and abundant vesicles, the periciliary region is easily identified in freeze-fracture replicas (Figs. 5–7). A prominent feature of the *periciliary vesicles* is a population of IMP ranging from 6 to 13 nm in diameter. The size distribution of IMP in PF leaflets is unimodal (Fig. 8) with a mean IMP size of 9.9 ± 0.2 nm and a density of 1,921 ± 122/μm^2. The EF leaflet has a similar size distribution of IMP, but a much lower density (Table I). In addition to the abundant vesicles with prominent IMP, we have occasionally observed smooth membrane profiles (Fig. 5) and cup-like profiles (Fig. 6), neither of which contain large numbers of IMP.

The size distribution of IMP of periciliary vesicles is similar to that found in endoplasmic reticulum and Golgi complex (Figs. 8–10). The latter membranes were analyzed exclusively in the myoid region of the inner segment; the region intervening between nucleus and the mitochondria-rich ellipsoid. Endoplasmic reticulum (mostly RER) was identified on the basis of its arrangement in the form of extensive parallel cisternae (Fig.

9). Relatively small regions of SER are found in sectioned material, particularly near the nucleus and the ellipsoid region, but such regions are indistinguishable from RER in replicas and, as a consequence, may contribute to the data. Golgi regions were identified on the basis of the fenestrated appearance of Golgi sacs with surrounding vesicles (Fig. 10). The IMP of PF leaflets of both endoplasmic reticulum and Golgi complex had a size distribution like that of the periciliary vesicles (Fig. 8). The IMP density, however, averaged, respectively, 35 and 24% higher than in vesicles (Fig. 8).

IMP size in the inner segment plasma membrane of the immediate periciliary region was similar to that in vesicles, cilium, and ROS (see below). In the remainder of the inner segment plasma membrane, however, IMP were significantly ($P \leq 0.01$) smaller in size (Figs. 8, 9, 11, 12, and 15). Here IMP sizes were distributed as a unimodal distribution ranging from 5 to 12 nm in size with an average size of 7.6 ± 0.1 and an average density ~55% greater than in the vesicles (Fig. 8). In addition, the IMP density of the inner segment plasma membrane was only about two-thirds that found in the outer segment (compare in Figs. 11, 12, and 15). Thus, inner segment plasma membrane is clearly distinguishable from both cytoplasmic membranes of the inner segment and ROS membranes. The characteristic size distribution of IMP in the inner segment applies to the calycal processes as well (Figs. 1, 11, and 15). These structures extend from the inner segment to surround the outer segment but do not establish direct membrane continuity with the ROS. The average IMP size in calycal processes was not significantly different ($P \geq 0.1$) from that found in the remainder of the inner segment plasma membrane, but the IMP density averaged 18% higher (Table II).

The differences between membranes of the inner segment noted above cannot be accounted for as differential partitioning of IMP between PF and EF leaflets (Table I). The EF leaflets consistently had far fewer IMP than corresponding PF leaflets (Figs. 5–10). The combined average IMP densities for PF and EF leaflets lead to about the same proportional differences in densities among the membrane compartments (Table I). Furthermore, we have analyzed the size distribution of IMP for each EF leaflet and in each case find unimodal distributions with an average IMP size not significantly ($P \leq 0.05$) different from those found in corresponding PF leaflets.

Membranes of the Outer Segment

ROS have been the subject of a number of freeze-fracture analyses carried out primarily to understand the structure of disc membranes (2, 13, 14, 25, 41, 44, 45). Such studies have consistently revealed in oblique fractures, a staircase arrangement of two fracture faces for each disc (Fig. 17). It is widely thought that the IMP-rich face corresponds to the cytoplasmic half of the lipid bilayer (PF leaflet) and the IMP-poor face corresponds to the intradiscal half of the bilayer (EF leaflet; see Figs. 16 and 17).[2] Longitudinally fractured ROS reveal, in addition to cross-fractured discs, incisures that extend from the disc margins toward their centers (Figs. 1 and 13). Large-shadowed structures are often visible along the incisure edge of each disc (see Fig. 13, and reference 44) which may corre-

---

[2] Despite the contrary opinion that fractures occur at membrane surfaces (44, 45), we follow the analysis and data of Corless et al. (14) which are best interpreted in terms of lipid bilayer splitting. As a consequence, conventional terminology for labeling fracture faces is used.
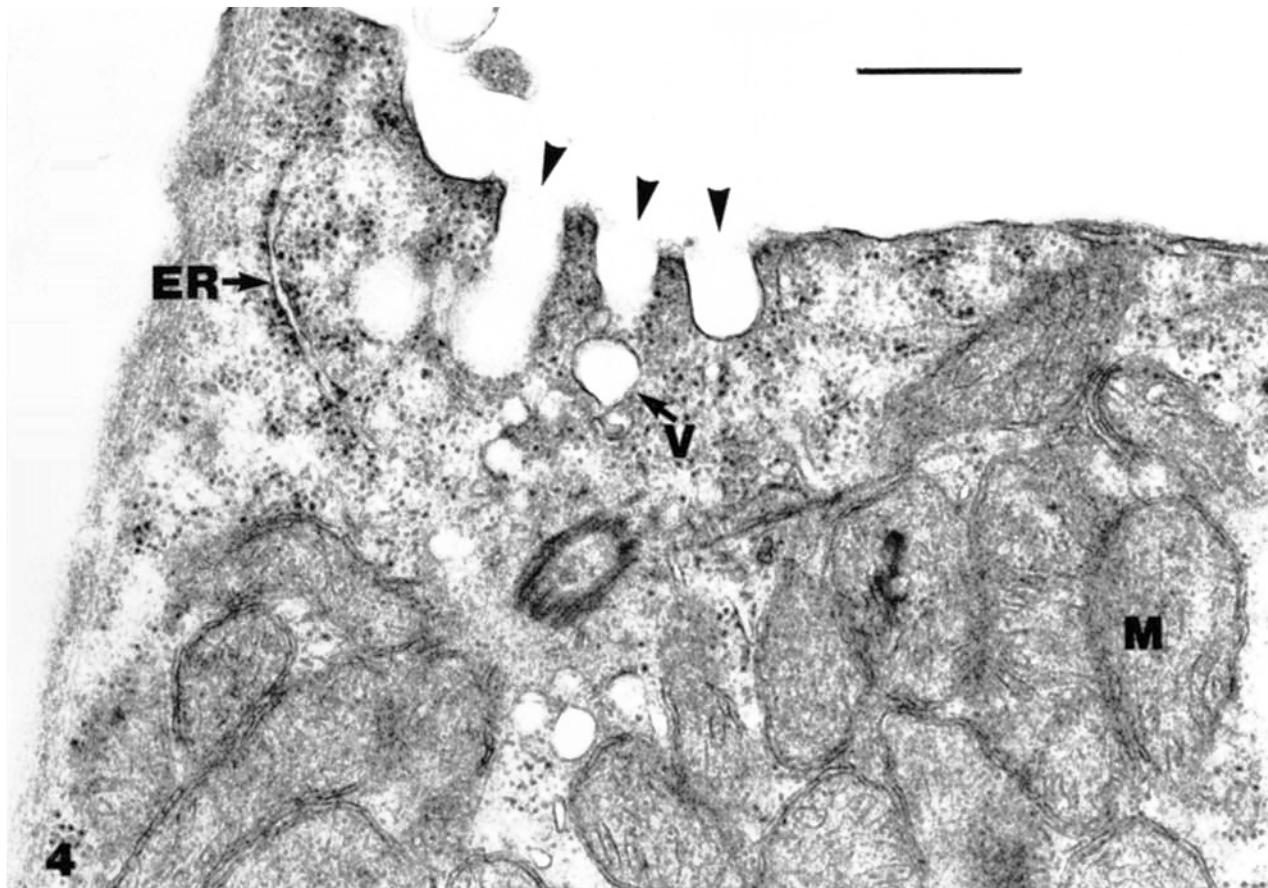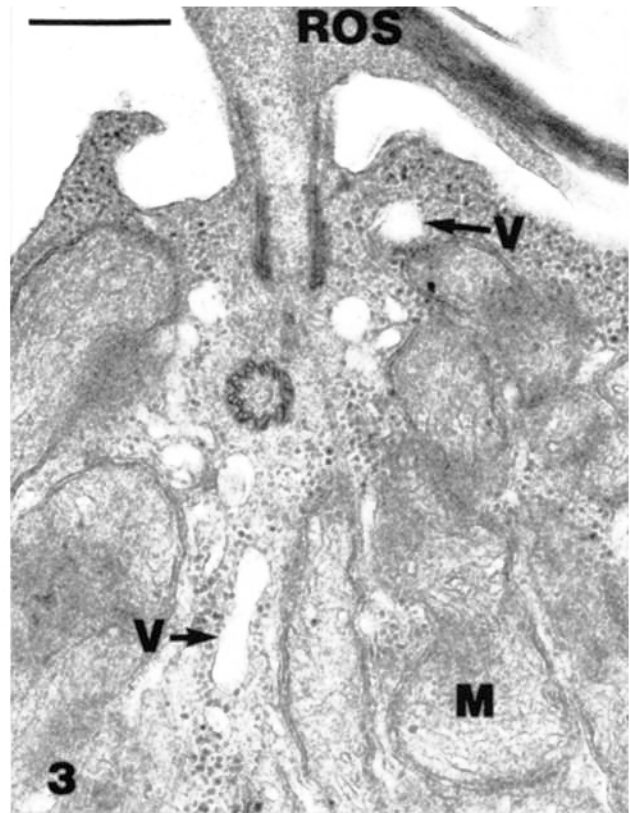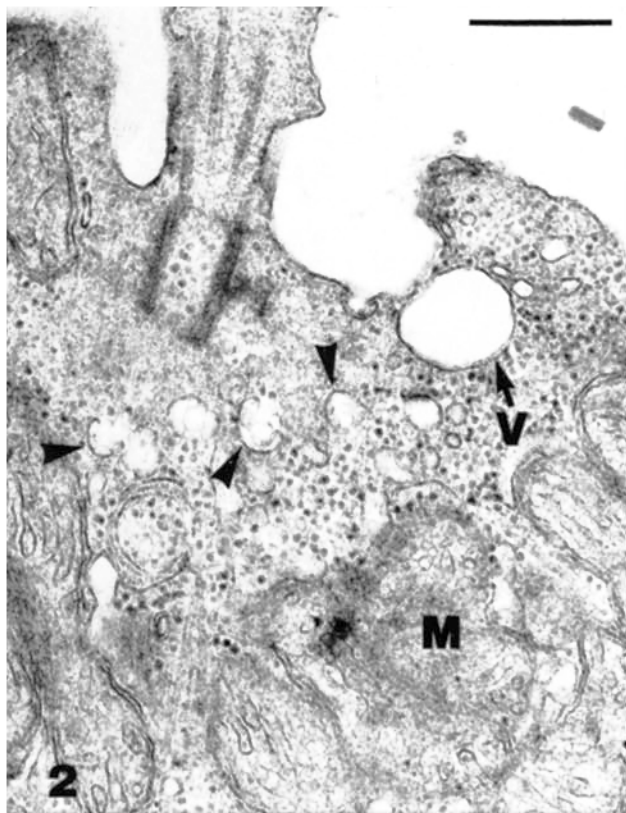
spond to the high molecular weight intrinsic protein recently localized to the incisure region using immunocytochemical techniques (38). The ROS plasma membrane is similar in structure to discs (compare Figs. 11 and 13 to 17), revealing uniformly distributed IMP with a size and density similar to that within discs (Fig. 8).

Quantitative analysis of the IMP within the ROS revealed a great similarity of structure throughout the system. IMP ranged in size from 7 to 14 nm with size distributions best characterized as unimodal with an average size near 10 nm (Fig. 8). The size distribution of IMP was not significantly different ($P \leq 0.01$) throughout the ROS. Likewise, IMP densities in ROS plasma membrane, basal ROS discs, and discs in approximately the middle and distal thirds of the ROS did not vary significantly (Fig. 8). A major qualification to this observation, however, relates to the occasional appearance of IMP-free areas in PF leaflets in ROS membranes. Previous studies have revealed IMP-free areas in the ROS plasma membrane of rats, guinea pigs, and frogs (2, 23, 42, 45), and recent observations have indicated that similar IMP-free areas are present in basal discs near the frog inner segment (2). Despite extensive searching we have not seen IMP-free areas in the ROS plasma membrane, but have detected small IMP-free areas in some replicas of basal disc membranes and ciliary plasma membrane. In the region immediately surrounding IMP-free areas IMP density was like that throughout the remainder of the ROS. Because of their rarity in our replicas IMP-free areas had little influence on the quantitative analysis (Fig. 8). Although the average IMP densities tended to be somewhat lower in basal discs and cilium, the differences were not statistically significant.

Differences between the plasma membranes of inner and outer segments were not caused by differential partitioning of IMP between the two membrane leaflets (Table I). Throughout the inner segment IMP densities on the EF leaflet ranged from 350–440 IMP/μm^2 and their average size was not significantly different from that of IMP found on the PF leaflet of each membrane system. Compared to the inner segment, ROS plasmalemma exhibited fewer IMP on the EF leaflet, but this difference could not account for the much greater PF leaflet density in the outer segment as is indicated by the number of IMP on the two leaflets combined (Table I).

Plasma Membrane of the Connecting Cilium and Periciliary Region

Inner and outer segments are connected by a short, nonmotile cilium (Figs. 1–3 and 14). The ciliary plasmalemma, identified in replicas as a region of membrane continuity between inner and outer segments, was rarely detected in our material

TABLE I

Density of IMP in PF and EF Leaflets of Rod Photoreceptor Membranes

Membrane	PF	EF	PF + EF	EF/PF
	IMP/μm^2			
Inner Segment				
Plasma membrane	2,976 ± 79	395 ± 40	3,371	0.13
Endoplasmic reticulum	2,598 ± 164	420 ± 34	3,018	0.16
Golgi complex	2,390 ± 90	338 ± 50	2,728	0.14
Periciliary vesicles	1,921 ± 122	300 ± 51	2,221	0.16
Outer Segment				
Plasma membrane	4,485 ± 65	250 ± 43	4,735	0.06
Basal discs	4,479 ± 123	263 ± 50	4,742	0.06
Middle discs	4,629 ± 63	281 ± 44	4,910	0.06
Apical discs	4,530 ± 75	227 ± 31	4,757	0.05

Data for PF are the same as those presented in Fig. 8. Note that the EF leaflet of inner segment membranes contains a greater fraction of the IMP than the ROS membranes. Note also that the average IMP densities for EF leaflets of Golgi complex and vesicles are not significantly different from those in the ROS.

(Fig. 14). In those cases where the ciliary PF leaflet was visible, IMP size distributions were indistinguishable from those found in the ROS (Fig. 8). Furthermore, IMP with the same size characteristics extended for some distance into the inner segment plasma membrane of the periciliary region (Fig. 14). These observations corroborated data in previously published micrographs; replicas of rat ROS illustrated in the PF leaflets of the ciliary plasma membrane a dense population of IMP that was comparable to that within the discs (28, 42). However, the tendency for IMP of the PF leaflet of rat photoreceptors to be arranged in circumferential arrays (28) could not be detected in *X. laevis*. In some cases IMP appeared in linear arrays with intervening IMP-free areas (Fig. 14), but this was not a regular feature of the cilium.

Similarity of Rods and Cones

The retina of *X. laevis* contains both rods and cones, and as far as possible we have obtained data on cone photoreceptors paralleling those described above for rods. Cones are easily distinguished from rods by the presence of a large oil droplet in the ellipsoid region of the inner segment (Fig. 18). In both tissue sections and replicas, vesicles similar in structure to those of rods are visible near the COS and are particularly prominent near the base of the calycal processes and connecting cilium (Fig. 19). In addition, COS discs have abundant, uniformly distributed IMP (Fig. 20). Comparison of IMP size distribu-

---

FIGURES 2–4 Electron micrographs illustrating periciliary vesicles (V) of thin-sectioned photoreceptors. Calibration bars of all figures in this paper correspond to 0.5 μm.

FIGURE 2 Section through the cilium illustrating a large vesicle (V) in close apposition to the plasma membrane. In addition to small vesicles seen adjacent to the large vesicle and among mitochondria (M), there are several cup-like vesicles (arrowheads). × 37,300.

FIGURE 3 Membrane vesicles and cisternae near the basal body and cilium. Discs of the ROS are seen above. × 37,300.

FIGURE 4 Section through the region adjacent to the cilium (note the presence of a centriole) illustrating vesicles (V) and a cisterna of rough endoplasmic reticulum (ER). Deep depressions in the cell surface (arrowheads) may be sites where vesicles fuse with the plasma membrane. Depressions like this are consistently found in sections adjacent to the cilium, and can be used to identify the periciliary region in sections and replicas. × 42,700.
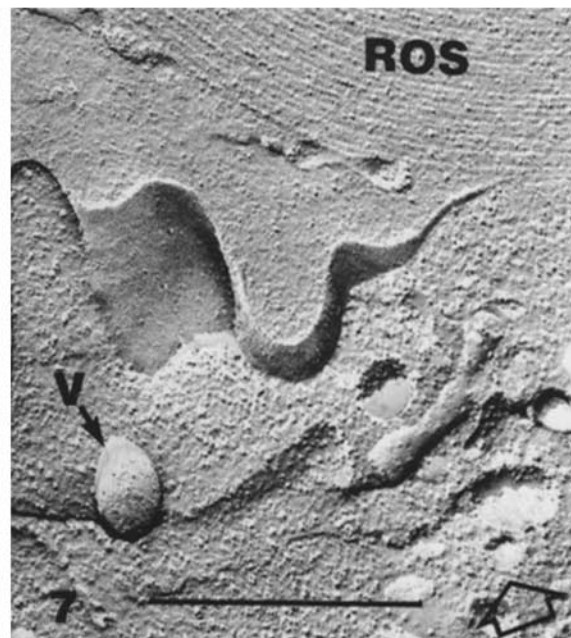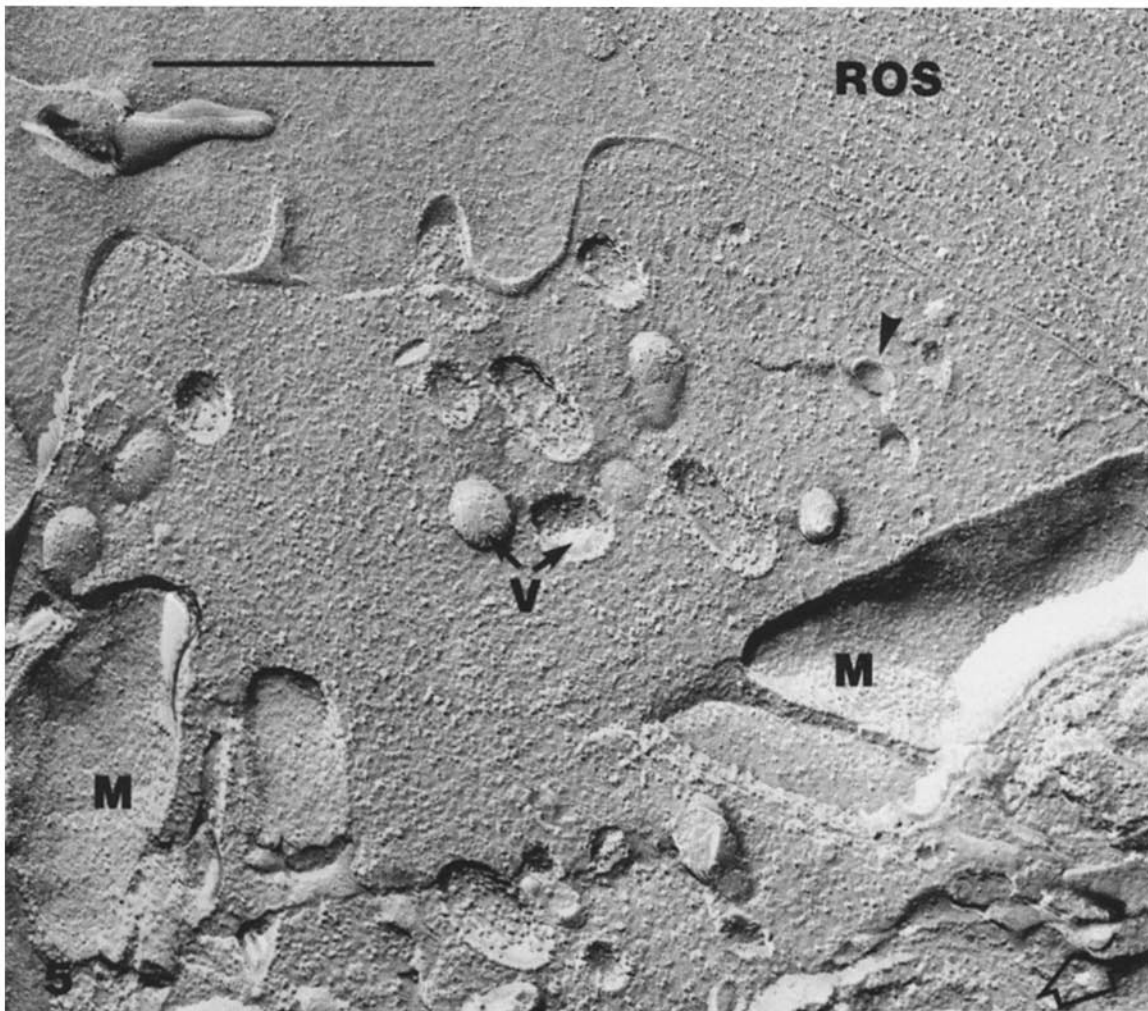
FIGURES 5–7   Electron micrographs of freeze-fracture replicas illustrating cytoplasmic vesicles (V) in the inner segment, adjacent to the outer segment (ROS). Open arrows indicate direction of shadowing. Shadows on replicas are white.

FIGURE 5   Micrograph illustrating both concave (PF) and convex (EF) vesicle profiles above and between mitochondria (M), as well as adjacent depressions in the plasma membrane. In addition to IMP-rich vesicles (V) occasional profiles of small IMP-poor membrane (arrowhead) are seen. × 75,000.

FIGURE 6   Micrograph illustrating characteristic periciliary vesicles (V) as well as cup-like profile (arrowhead). × 75,000.

FIGURE 7   Micrograph illustrating the EF leaflet of a vesicle (V) and adjacent depression in the inner segment plasma membrane. × 67,250.

tions (Table II) indicate that the two photoreceptor types are very similar. However, we consistently observed ~12% fewer IMP in inner segment plasma membrane and calycal processes than in comparable structures in rods. Nonetheless, it should be emphasized that the general conclusions of this analysis apply to rod and cone photoreceptors alike.

DISCUSSION

Outer Segment Membranes in Rods and Cones

The ROS membrane system is relatively simple in that its predominant intrinsic membrane protein is visual pigment (17), a glycoprotein (18) that contains two asparagine-linked oligosaccharide chains (16). In several systems visual pigment apoprotein has been found to make up 80–85% of ROS membrane protein (9, 17, 19). Visual pigment is an intrinsic component of both discs and ROS plasma membrane (3, 23) where it gives rise to a relatively uniform distribution of IMP with a density of ~4,500–6,000/μm^2 in PF leaflets (2, 13, 14, 25, 27, 41). The IMP distribution in ROS probably reflects the presence of visual pigment within the lipid bilayer, because a similar freeze-fracture picture is obtained from artificial lipid bilayers containing rhodopsin (11, 12, 22). Estimates of the number of rhodopsin molecules per square micrometer of disc membrane, however, are generally four to five times higher than the number of IMP (12, 14), indicating that the IMP and rhodopsin do not correspond on a one-to-one basis (14, 25). Apparently, each IMP represents an aggregate of visual pigment molecules. Because available x-ray diffraction data indicate that rhodopsin is not aggregated in the native membrane (10), it has been suggested that the IMP distribution arises through aggregation and plastic deformation of visual pigment molecules during rapid freezing and fracturing (13, 14).

In *X. laevis* a distribution of IMP in ROS membranes similar to that observed in other species is evident. In attempting to compare membranes in different regions of the outer segment we have found remarkable uniformity throughout. Thus, the size and density of IMP was not significantly different in comparisons of basal discs, middle discs, apical discs, and ROS plasma membrane (see Fig. 8). Our observations contrast with previous reports of extensive IMP-free areas in ROS plasma membrane and basal discs of mice, rats, and frogs (2, 23, 45). We have not seen IMP-free areas in ROS plasma membrane but have seen small IMP-free areas in basal discs and ciliary plasma membrane. Because of their rarity in our replicas, IMP-free areas had a negligible effect in reducing overall IMP densities in the basal ROS and cilium.

An important observation of the present study is a great similarity of rod and cone photoreceptors in the distribution of IMP sizes and densities. In the inner segment plasma membrane, cytoplasmic vesicles, and outer segment of cones we found IMP size distributions indistinguishable from those of comparable membranes in rods. Furthermore, we have found that IMP densities of cone cytoplasmic vesicles and outer segments are indistinguishable from those in rods, and have failed to detect IMP-free areas in cone outer segments including those discs adjacent to the inner segment. Although not reported in previous freeze-fracture studies, the similarity of rods and cones is not surprising. The cone visual pigment is apparently based on an apoprotein component similar to rod opsin (46) which turns over as a part of the outer segment membrane system (1). In view of the similarities in membrane structure, we suggest that the basic model of disc assembly developed in
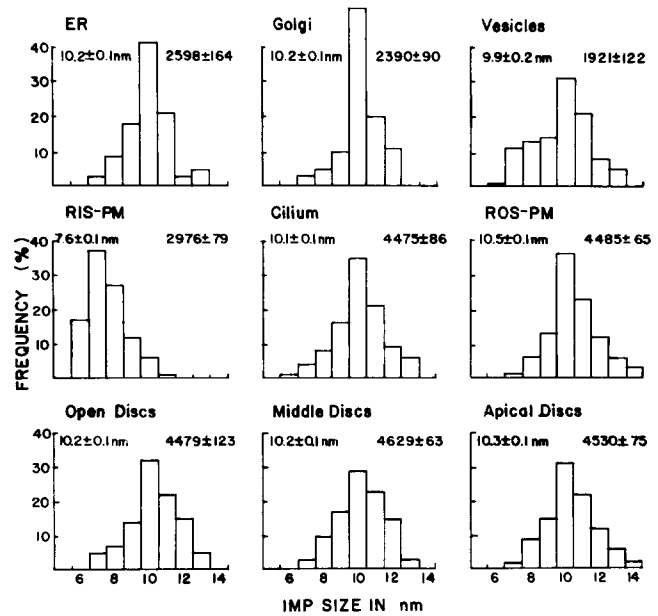

FIGURE 8 Size frequency histograms illustrating the size distribution in PF leaflets of IMP in membrane systems along the putative renewal pathway of ROS membranes. Along with each histogram the average (mean ± standard error) IMP size and density are given on the left and right sides, respectively. Data for open discs were obtained from discs identified as being within 15 discs of the inner segment. Data for middle and apical discs were from roughly the middle and distal third of the ROS, respectively.

this paper (see below) for ROS applies to cone photoreceptors as well.

Cytoplasmic Membranes of the Inner Segment

In the present analysis we have examined IMP size and density in inner segment and ciliary membranes with the object of comparing them directly to the IMP populations observed in the ROS membranes. The value of the comparisons is highly dependent on the accuracy of our determination of the size frequency distributions and on the functional significance of identity in size of IMP in different membrane systems. Measurements of IMP size are complicated by the fact that several factors other than the actual diameter of the intrinsic membrane component contribute to the size observed in a freeze-fracture replica (29). For example, thickness of the carbon-platinum replica, local shadowing angle when irregular membrane surfaces deviate from horizontal, surface contamination before replication, variations in the degree of etching, and plastic deformation of intrinsic membrane components during fracture may each influence an IMP's apparent size. Each of these, with the possible exception of plastic deformation can be controlled, however, making it possible to use the overall size frequency distribution of IMP for comparison of different membranes. The facts that (a) we consistently observed the size differences within a single replica and in many cases within a single cell (cf. Fig. 15), (b) replica thickness was carefully controlled so that variations in IMP size within the same membrane compartments in different replicas was negligible, and (c) that specimen contamination was reduced by working in an excellent vacuum convince us that the observed size distributions are valid and comparable characterizations of the different membrane systems.
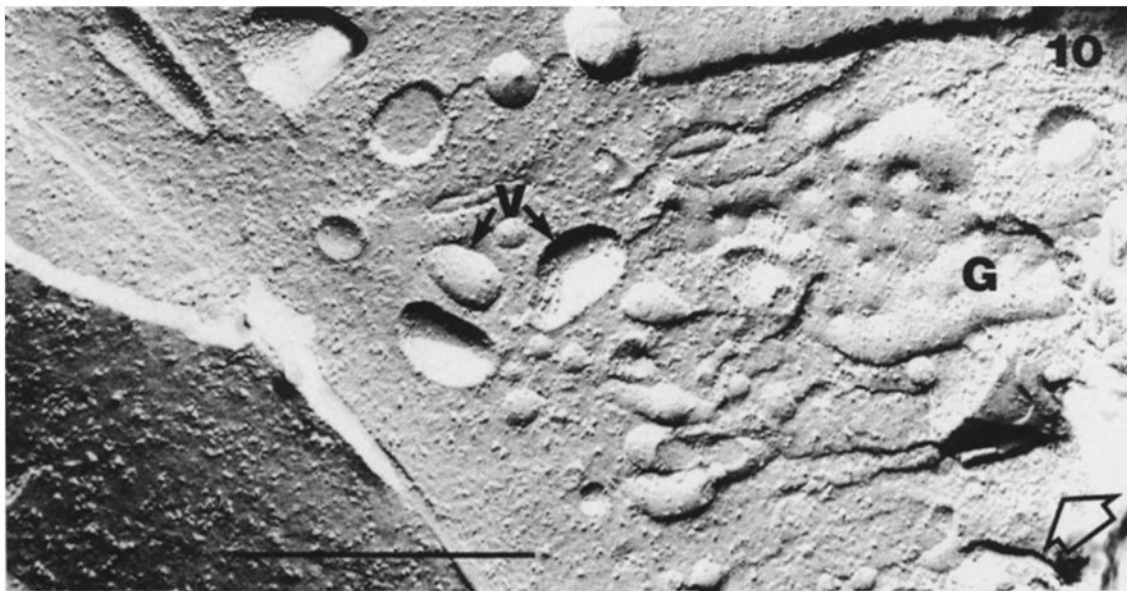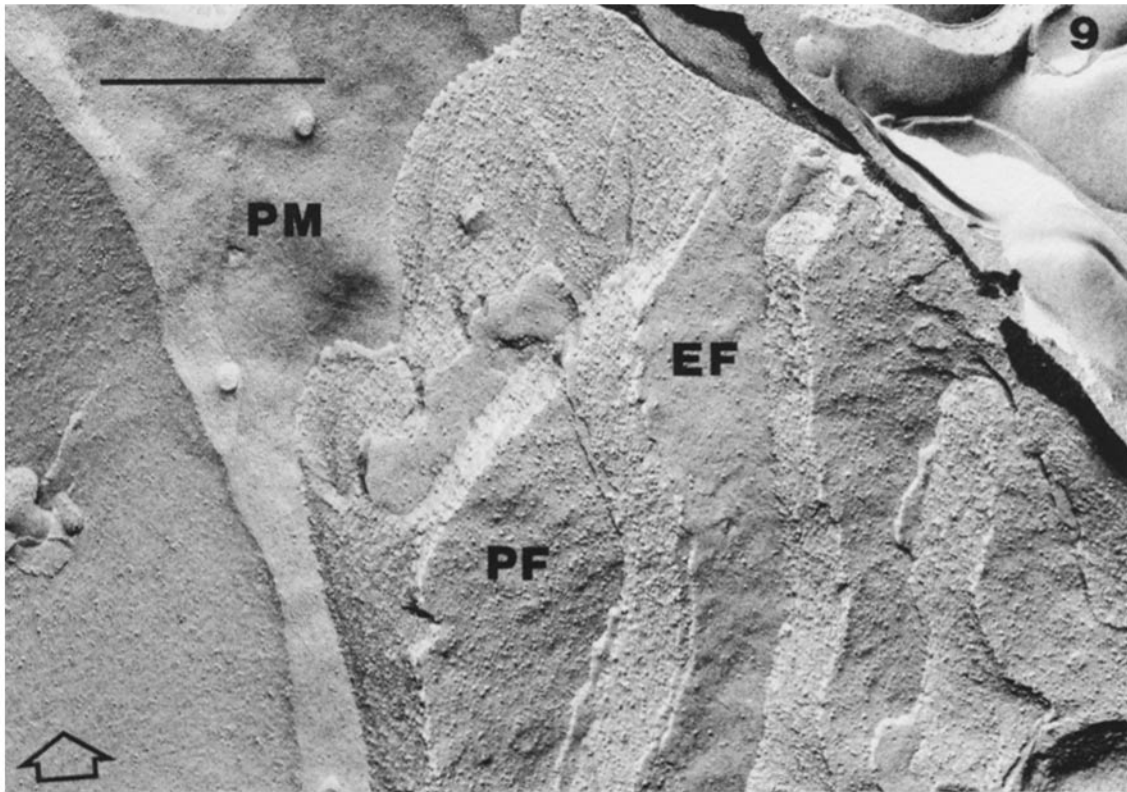
FIGURES 9 and 10 Electron micrographs of freeze-fracture replicas illustrating endoplasmic reticulum and Golgi complex (G).

FIGURE 9 Micrograph illustrating the EF leaflet of the inner segment plasma membrane (PM) as well as PF and EF leaflets of elongated cisternae of endoplasmic reticulum. × 59,700.

FIGURE 10 Micrograph illustrating the Golgi complex (G; EF leaflet) and surrounding vesicles (V; EF and PF leaflets) in the inner segment myoid region. × 80,000.

FIGURES 11–15 Electron micrographs of freeze-fracture replicas illustrating the inner and outer segment plasma membrane.

FIGURE 11 Micrograph illustrating cross-fractured discs (D), the EF leaflet of the ROS plasma membrane and the PF leaflet (lower center) of an adjacent ROS. Note the presence of calycal processes (C) adjacent to the ROS. × 45,125.

FIGURE 12 Micrograph illustrating the PF leaflet of the rod inner segment plasma membrane. Note the smaller size and lower density of IMP compared to those in the ROS plasma membrane (Fig. 11). × 45,125.

FIGURE 13 Micrograph illustrating the ROS plasma membrane (PM) enclosing cross-fractured discs. An incisure runs parallel to the plasma membrane and between the arrows exhibits large shadowed structures at the incisure edge of discs. × 48,900.

FIGURE 14 Micrograph illustrating the PF leaflet of the ciliary plasma membrane and adjacent inner segment (IS). Note the small IMP-free areas in both inner segment and ciliary membrane. × 85,000.

FIGURE 15 Micrograph illustrating the PF leaflets of membrane of outer segment (OS), adjacent inner segment (IS), and calycal processes (C). Note the striking differences in IMP populations. × 85,000.
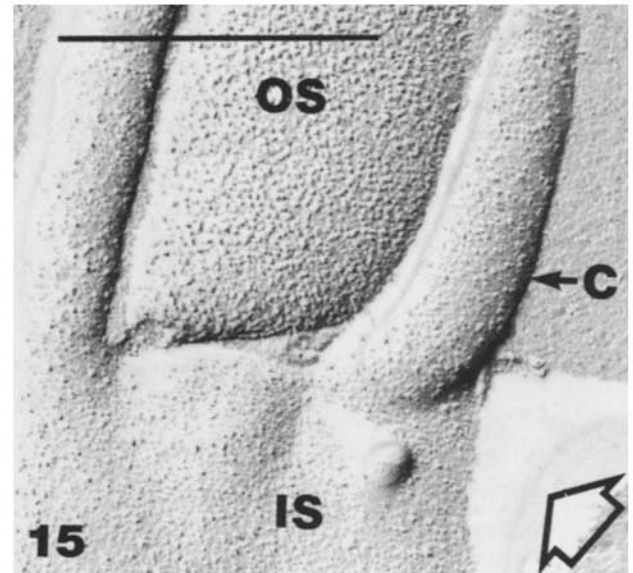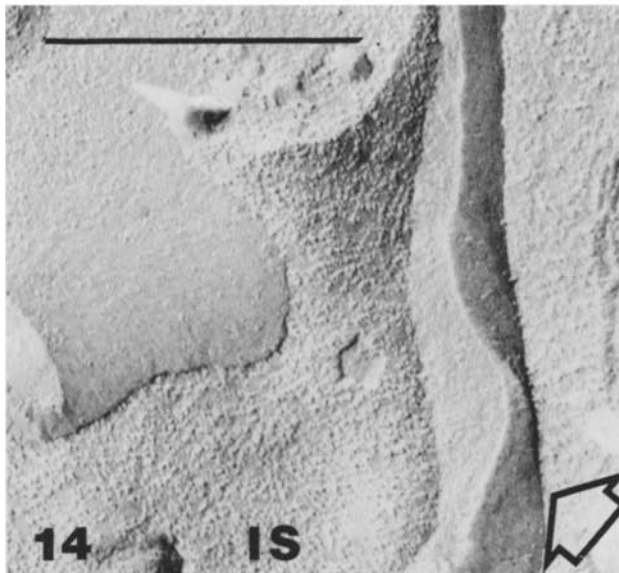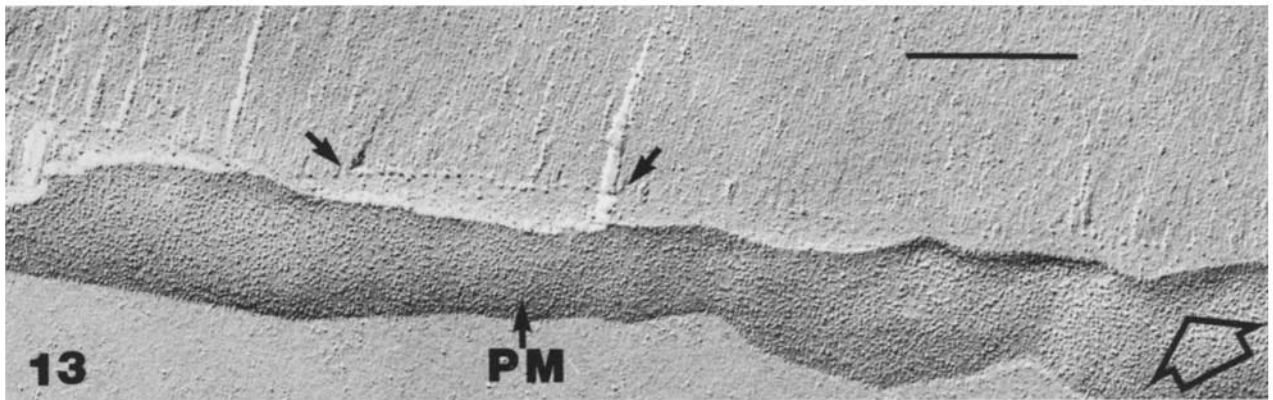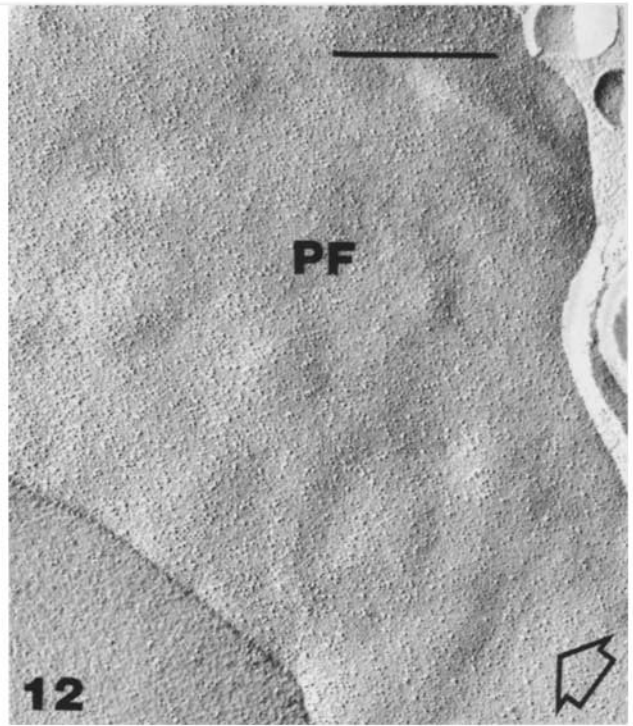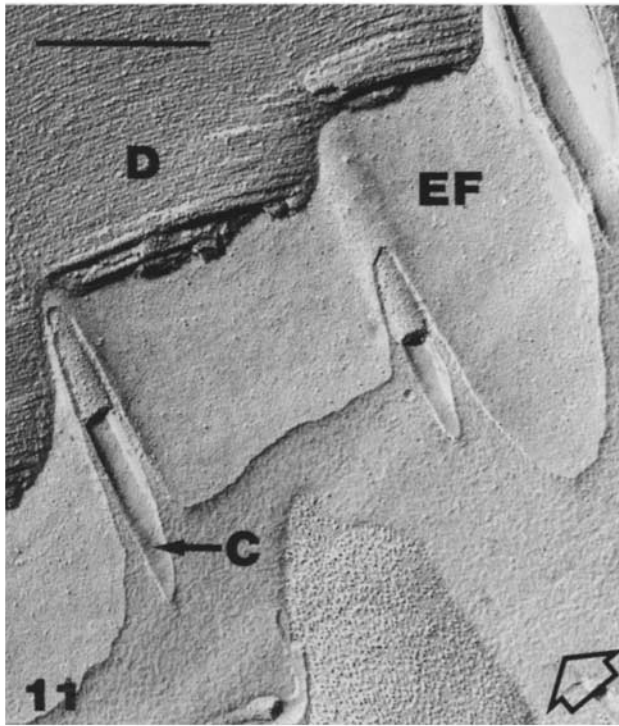
TABLE II

Comparison of Mean Density and Size of IMP in the PF Leaflet of Membranes of Rod and Cone Photoreceptors

Membrane	Rod	Cone	Mean IMP size	
			Rod	Cone
	IMP/μm^2		nm	
Inner segment plasma membrane	2,989 ± 81	2,627 ± 86	7.6 ± 0.12	7.9 ± 0.14
Calycal processes*	3,523 ± 161	3,092 ± 203	7.5 ± 0.12	7.4 ± 0.11
Discs‡	4,629 ± 63	4,613 ± 86	10.2 ± 0.14	10.1 ± 0.15
Periciliary vesicles	1,921 ± 121	2,050 ± 239	9.9 ± 0.16	9.7 ± 0.15

Data are from size frequency distributions like those in Fig. 8. Note that the IMP density is greater in calycal processes and discs than in the inner segment and that mean IMP size is greater in discs and vesicles than in inner segment plasma membrane as well as calycal processes.

* An extension of the inner segment plasma membrane as illustrated in Figs. 1, 11, 15, and 18.

‡ Average for discs throughout the ROS.

The basic conclusion from our comparison of inner and outer segment membranes is that IMP of cytoplasmic membranes of the inner segment have a size distribution similar to that of ROS membranes and unlike that of the inner segment plasma membrane. IMP density, however, is lower throughout the inner segment than in the cilium and ROS membranes. For each membrane system analyzed, we have observed a unimodal distribution of IMP sizes. Statistical analysis indicates that with the exception of the inner segment plasma membrane where IMP are smaller in size, the size distributions are not significantly different from each other. Such observations are consistent with the suggestion (4, 21, 24) that a precursor-product relationship exists between endoplasmic reticulum, Golgi and vesicle membranes of the inner segment and ROS membranes.

In photoreceptors opsin is a major intrinsic protein and is likely to be the basis for IMP of 10 nm average size on PF leaflets in ROS. Therefore, it is possible that IMP of similar size represent a marker for membrane destined for the ROS, even though IMP size in general is a relatively nonspecific parameter. Interpreted in terms of the assumption that IMP populations with a similar size distribution are identical or very similar, our observations suggest that, at the time of its synthesis, the visual pigment apoprotein becomes associated with cytoplasmic membranes and gives rise to IMP like those seen in the ROS. This hypothesis is consistent with data that indicate that protein destined for incorporation into outer segment membranes is synthesized in the RER of the myoid (51). Available evidence also suggests that glycosylation begins in RER and is continued in the Golgi region (8). Immunoreactive opsin is first detectable cytochemically in or near the Golgi complex (39) and cell fractionation studies indicate that opsin passes through the ellipsoid region in association with sedimentable membrane (35). Although these membrane systems undoubtedly play a role in processes other than opsin biosynthesis, available data suggests that opsin synthesis, processing, and transport all occur in association with cytoplasmic membranes.

Transition between Inner and Outer Segment Plasma Membrane and the Role of the Periciliary Region in Disc Renewal

IMP are generally smaller in size and fewer in number in the inner segment plasma membrane than in the ROS. In addition, less opsin is present in the inner segment plasma membrane (23). Further evidence for a difference between the two membranes comes from lectin-binding studies that show

that the number of ultrastructurally detectable concanavalin A, wheat germ agglutinin, and soybean agglutinin-binding sites is lower on the inner segment (33; J. C. Besharse, unpublished observation). The finding of major differences by both freeze-fracture and lectin binding between inner segment plasma membrane and ROS is hardly surprising in view of the differing functions of the two membrane systems. In contrast to the role of outer segment membranes in photon capture, the inner segment plasmalemma is thought to be the site of a ouabain-sensitive Na^+-K^+ ATPase that generates the photoreceptor dark current (48). Recent evidence indicates that [^{3}H]ouabain binds to the inner segment plasma membrane but not to that of the outer segment (7).

In favorable replicas of the connecting cilium, the characteristic IMP of the cilium spread for some distance onto the inner segment plasma membrane around the ciliary base. A similar spreading of large IMP around the ciliary base is evident in replicas of rodent photoreceptors as well (28, 42). Thus, segregation of the characteristic membrane domains of inner and outer segment occurs at the region around the ciliary base (i.e., periciliary region). The latter observation is relevant to the mechanism by which membrane is transported to newly forming discs. If many or all of the IMP seen in periciliary vesicles are destined for incorporation into the ROS, a potential mechanism for their transfer would be as follows: first, cytoplasmic vesicles fuse with the inner segment plasma membrane in the region adjacent to the cilium, and, subsequently, membrane or certain membrane components flow over the cilium into forming discs (see Fig. 1). This pathway for opsin transfer to the ROS is consistent with cytochemical observations indicating that immunoreactive opsin is present in the apical inner segment plasma membrane and cilium (23, 37), and with a hypothesis proposed on the basis of previous freeze-fracture analyses of the photoreceptor cilium (28, 42).

The difference in IMP density between vesicles and ROS discs raises a question regarding the fate of the excess lipid bilayer seen in vesicles. One possibility is that excess lipid bilayer may be retrieved from the surface through endocytosis. For example, horseradish peroxidase uptake has been demonstrated at the region of the ROS-inner segment junction (30). Although concentration of IMP may be compensated by retrieval and recycling of excess lipid bilayer, it must be emphasized that our own analysis of horseradish peroxidase uptake under conditions of light-evoked disc assembly in vitro (4) indicates that periciliary vesicles like those analyzed in this paper are not sites of uptake (J. C. Besharse and R. O. Terrill, manuscript in preparation). Another possibility is that excess
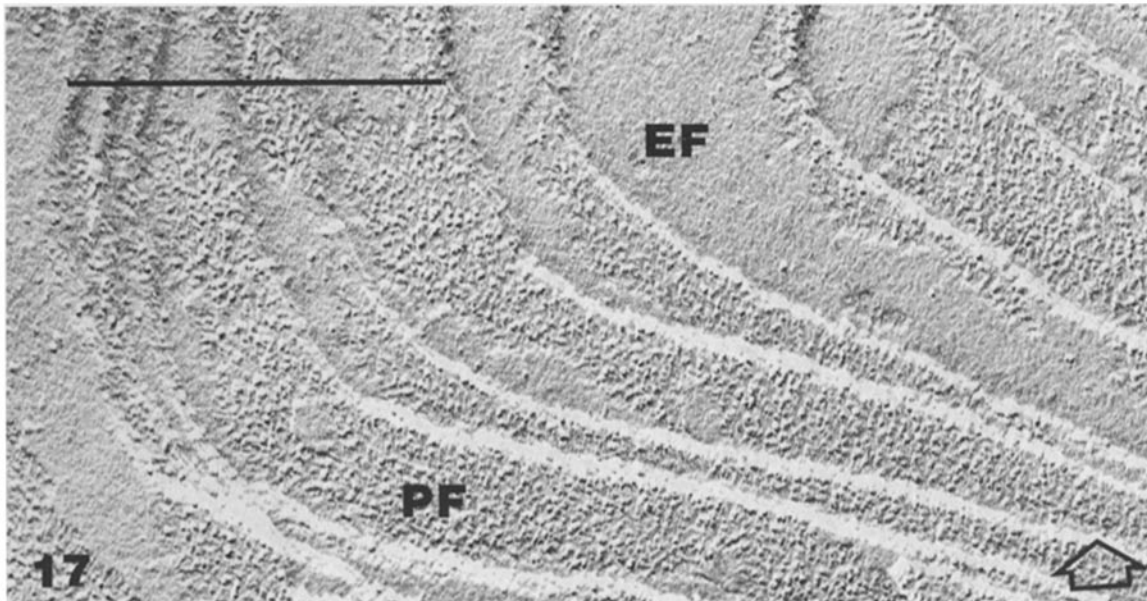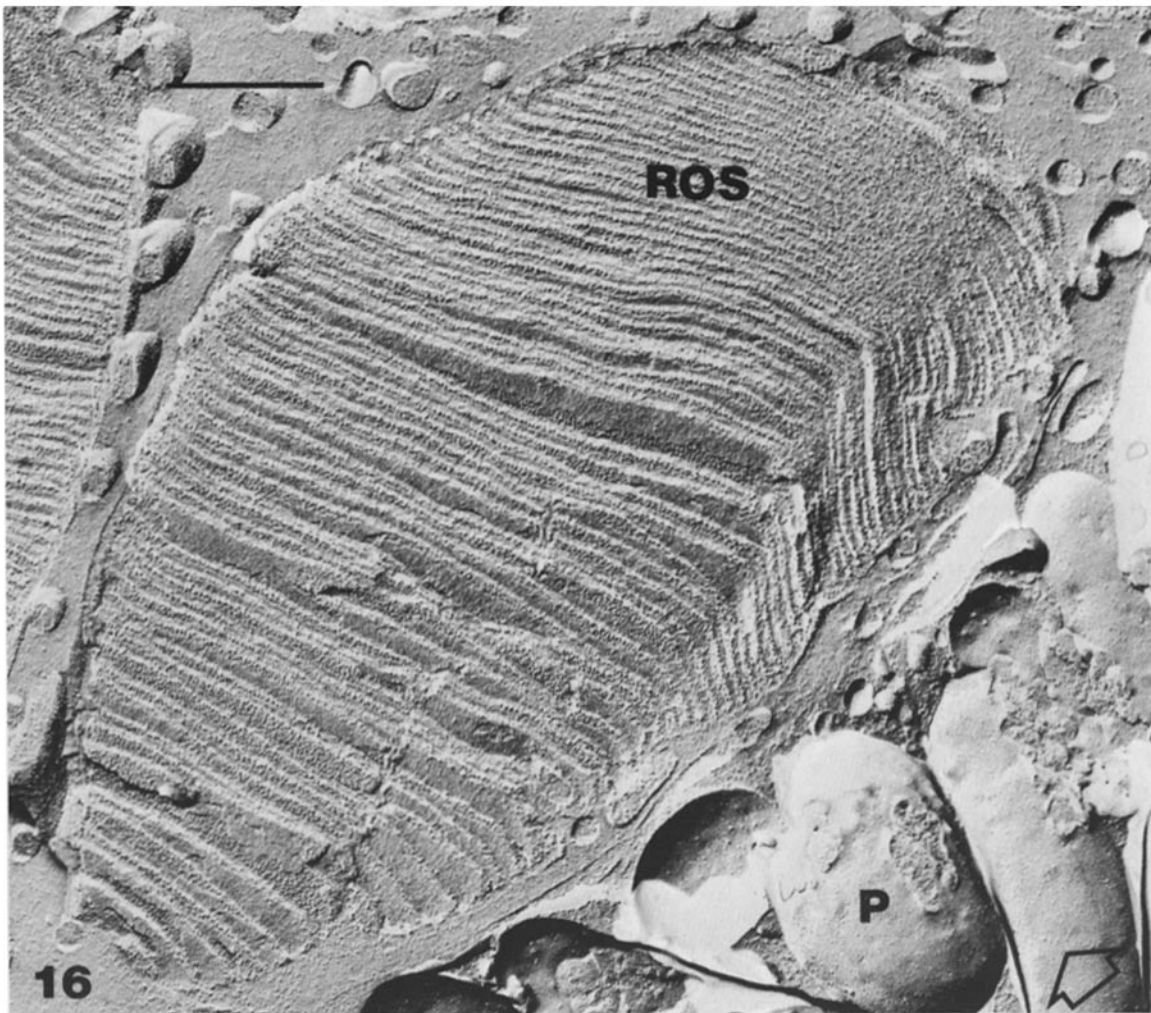
FIGURES 16 and 17   Electron micrographs of freeze-fracture replicas illustrating the structure of ROS disc membranes.

FIGURE 16   Micrograph illustrating an oblique fracture through an ROS and adjacent pigment epithelium (*P*). × 42,000.

FIGURE 17   Micrograph illustrating the alternating PF and EF leaflets of disc membranes. IMP are closely packed in PF leaflets but widely dispersed in EF leaflets. × 100,000.
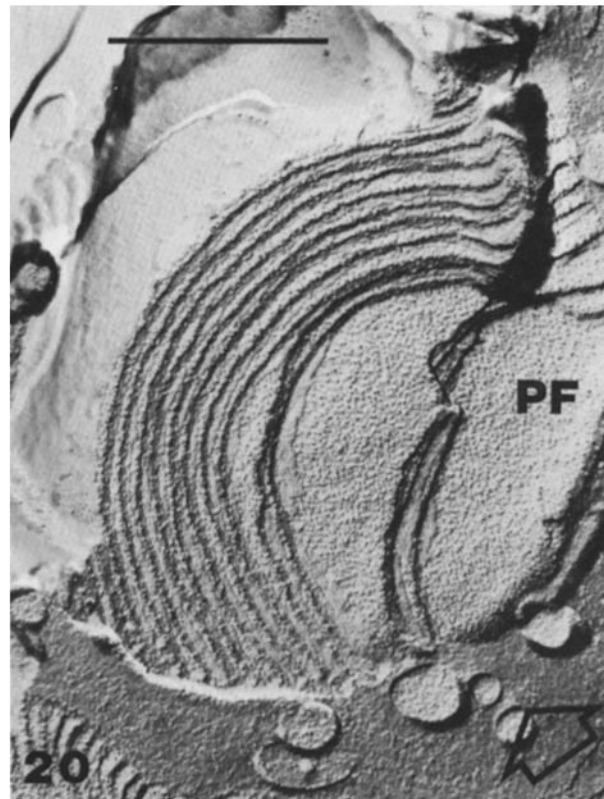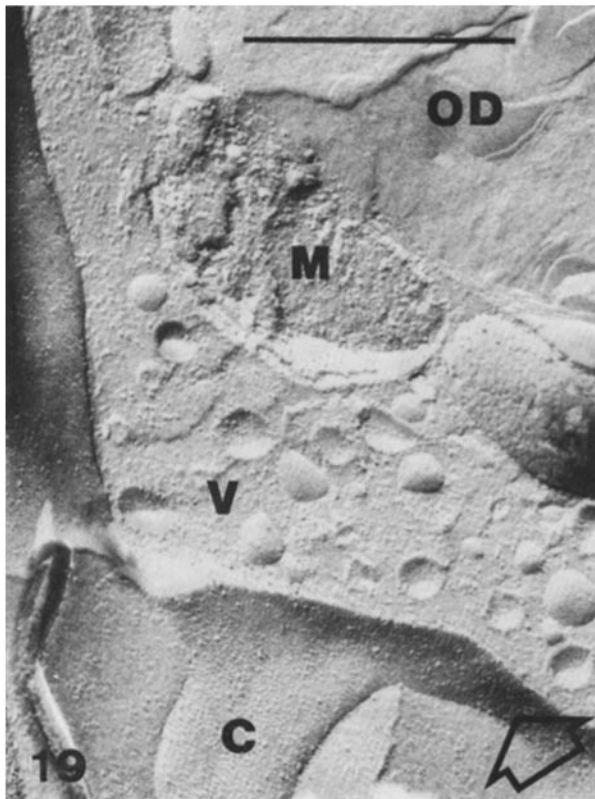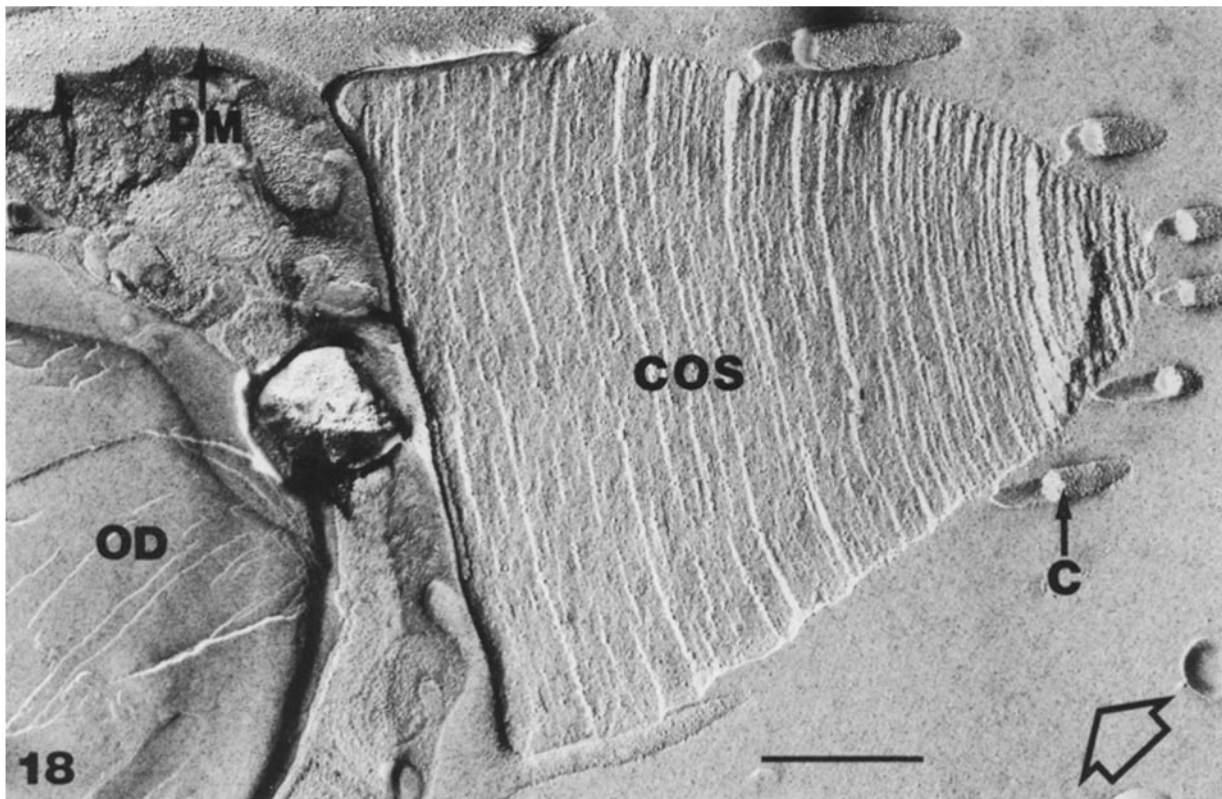
FIGURES 18–20   Electron micrographs of freeze-fracture replicas of cone photoreceptors.

FIGURE 18   Micrograph illustrating the conical outer segment (COS), the oil droplet (OD), inner segment plasma membrane (PM), and calycal processes (C) of a cone. × 42,900.

FIGURE 19   Micrograph illustrating cytoplasmic vesicles in a cone inner segment in the region adjacent to the apex of the inner segment. C, calycal process confluent with inner segment plasma membrane; OD, oil droplet, V, vesicles; M, mitochondrion. × 72,000.

FIGURE 20   Micrograph illustrating the structure of the PF and EF leaflets of conical outer segment disc membranes. × 58,700.

462

lipid bilayer may be transferred, at least in part, to the ROS, a view consistent with the frequent observation of IMP-free areas in ROS plasma membrane and basal discs (2). According to this mechanism IMP concentration (i.e., elimination of IMP-free areas) would occur within the ROS.

Although consistent with a variety of experimental observations on photoreceptors and with the general view that intrinsic membrane proteins remain associated with lipid bilayer from the time of their synthesis, evidence for the vesicle hypothesis described above is circumstantial. The hypothesis is subject, however, to a variety of experimental tests. For example, we have recently found evidence that vesicles like those described in this paper contain immunoreactive opsin (37). Furthermore, during a time when opsin labeled with radioactive amino acids is passing through the ellipsoid region of the inner segment in transit to the ROS, electron microscope autoradiography indicates that periciliary vesicles are heavily labeled (37). These observations as well as the lack of horseradish peroxidase uptake into periciliary vesicles are all consistent with a role for vesicles in membrane expansion in support of disc assembly.

REFERENCES

1. Anderson, D. H., S. K. Fisher, and R. H. Steinberg. 1978. Mammalian cones: disc shedding, phagocytosis, and renewal. *Invest. Ophthalmol. Visual Sci.* 17:117–133.
2. Andrews, L., and A. I. Cohen. 1979. Freeze-fracture evidence for the presence of cholesterol in particle free patches of basal discs and the plasma membrane of retinal rod outer segments of mice and frogs. *J. Cell Biol.* 81:215–228.
3. Basinger, S., D. Bok, and M. Hall. 1976. Rhodopsin in the rod outer segment plasma membrane. *J. Cell Biol.* 69:29–42.
4. Besharse, J. C. 1980. Light and membrane biogenesis in rod photoreceptors of vertebrates. *In* The Effects of Constant Light on Visual Processes. T. P. Williams and B. N. Baker, editors. Plenum Press, New York. 409–431.
5. Besharse, J. C., J. G. Hollyfield, and M. E. Rayborn. 1977. Photoreceptor outer segments: Accelerated membrane renewal in rods after exposure to light. *Science (Wash. D. C.).* 196:536–538.
6. Besharse, J. C., J. G. Hollyfield, and M. E. Rayborn. 1977b. Turnover of rod photoreceptor outer segments. II. Membrane addition and loss in relationship to light. *J. Cell Biol.* 75:507–527.
7. Bok, D., and B. Filerman. 1979. Autoradiographic localization of Na⁺-K⁺ ATPase in retinal photoreceptors and RPE with ³H-Ouabain. ARVO Abstracts. *Invest. Ophthalmol. Visual Sci.* 224. (Suppl.).
8. Bok, D., M. O. Hall, and P. O'Brien. 1977. The biosynthesis of rhodopsin as studied by membrane renewal in rod outer segments. *In* International Cell Biology 1976–1977. The Rockefeller University Press, New York. 608–617.
9. Bownds, D., A. Gordon-Walker, A. C. Guide-Huguenin, and W. Robinson. 1971. Characterization and analysis of frog photoreceptor membranes. *J. Gen. Physiol.* 58:225–237.
10. Chabre, M. 1975. X-ray diffraction studies of retinal rods. I. Structure of the disc membrane, effect of illumination. *Biochim. Biophys. Acta.* 382:322–335.
11. Chabre, M., A. Cavaggioni, H. B. Osborne, T. Gulik-Kryzwicki, and J. Olive. 1972. A rhodopsin-lipid-water lamellar system: its characterization by x-ray diffraction and electron microscopy. *FEBS (Fed. Eur. Biochem. Soc.) Lett.* 26:197–202.
12. Chen, Y. S., and W. L. Hubbell. 1973. Temperature- and light-dependent structural changes in rhodopsin-lipid membranes. *Exp. Eye Res.* 17:517–532.
13. Clark, A. W., and D. Branton. 1968. Fracture faces in frozen outer segments from the guinea pig retina. *Z. Zellforsch. Mikrosk. Anat.* 91:586–603.
14. Corless, J. M., W. H. Cobbs, III, M. J. Costello, and J. D. Robertson. 1976. On the

asymmetry of frog retinal rod outer segment disk membranes. *Exp. Eye Res.* 23:295–324.
15. Edwards, A. L. 1968. Experimental Design in Psychological Research. Holt, Rinehart and Winston, Inc. New York. 3rd Edition.
16. Fukuda, M. N., D. S. Papermaster, and P. Hargrave. 1979. Rhodopsin carbohydrate: Structure of small oligosaccharides attached at two sites near the amino terminus. *J. Biol. Chem.* 254:8201–8207.
17. Hall, M. O., D. Bok, and A. D. E. Bacharach. 1969. Biosynthesis and assembly of the rod outer segment membrane system. Formation and fate of visual pigment in the frog retina. *J. Mol. Biol.* 45:397–406.
18. Heller, J. 1968. Structure of visual pigments. I. Purification, molecular weight, and composition of bovine visual pigment. *Biochemistry* 7:2906–2913.
19. Heitzman, H. 1972. Rhodopsin is the predominant protein of rod outer segment membranes. *Nat. New Biol.* 235:114.
20. Hirano, H., B. Parkhouse, G. L. Nicolson, E. S. Lennox, and S. J. Singer. 1972. Distribution of saccharide residues on membrane fragments from a myeloma-cell homogenate: its implications for membrane biogenesis. *Proc. Natl. Acad. Sci. U. S. A.* 69:2945–2949.
21. Holtzman, E., S. Schacher, J. Evans, and S. Teichberg. 1977. Origin and fate of membranes of secretion granules and synaptic vesicles: membrane circulation in neurons, gland cells and retinal photoreceptors. *In* The Synthesis, Assembly and Turnover of Cell Surface Components. G. Poste and G. L. Nicolson, editors. Elsevier North-Holland, New York. 165–246.
22. Hong, K., and W. Hubbell. 1972. Preparation and properties of phospholipid bilayers containing rhodopsin. *Proc. Natl. Acad. Sci. U. S. A.* 69:2617–2621.
23. Jan, L. Y., and J.-P. Revel. 1974. Ultrastructural localization of rhodopsin in the vertebrate retina. *J. Cell Biol.* 62:257–273.
24. Kinney, M. S., and S. K. Fisher. 1978. The photoreceptor and pigment epithelium of the larval *Xenopus* retina: morphogenesis and outer segment renewal. *Proc. R. Soc. Lond. Biol. Sci.* 201:149–167.
25. Krebs, W., and H. Kühn. 1977. Structure of isolated bovine rod outer segment membranes. *Exp. Eye Res.* 25:511–526.
26. LaVail, M. M. 1973. Kinetics of rod outer segment renewal in the developing mouse retina. *J. Cell Biol.* 58:650–661.
27. Leeson, T. S. 1970. Rat retinal rods: freeze-fracture replication of outer segments. *Can. J. Ophthalmol.* 5:91–107.
28. Matsusaka, T. 1974. Membrane particles of the connecting cilium. *J. Ultrastruct. Res.* 48:305–312.
29. McNutt, N. S. 1977. Freeze-fracture techniques and applications to the structural analysis of the mammalian plasma membrane. *Cell Surf. Rev.* 3:75–126.
30. Mercurio, A. M., and E. Holtzman. 1979. Agranular reticulum and membrane biogenesis in *Rana pipiens* photoreceptors. *J. Cell Biol.* 83 (2, Pt. 2): 136a (Abstr.).
31. Nieuwkoop, P. D., and J. Faber. 1967. Normal Table of *Xenopus laevis* (Daudin). North-Holland Publishing Co., Amsterdam. 245.
32. Nilsson, S. E. G. 1964. Receptor cell outer segment development and ultrastructure of the disk membranes in the retina of the tadpole *(Rana pipiens). J. Ultrastruct. Res.* 11:581–621.
33. Nir, I., and M. O. Hall. 1979. Ultrastructural localization of lectin binding sites on the surface of retinal photoreceptors and pigment epithelium. *Exp. Eye Res.* 29:181–194.
34. Palade, G. 1975. Intracellular aspects of the process of protein synthesis. *Science (Wash. D. C.).* 189: 347–358.
35. Papermaster, D. S., C. A. Converse, and J. Siu. 1975. Membrane biosynthesis in the frog retina: opsin transport in the photoreceptor cell. *Biochemistry.* 14:1343–1352.
36. Papermaster, D. S., C. A. Converse, and M. Zorn. 1976. Biosynthetic and immunochemical characterization of a large protein in frog and cattle rod outer segment membranes. *Exp. Eye Res.* 23:105–115.
37. Papermaster, D. S., B. G. Schneider, and J. C. Besharse. 1979. Assembly of rod photoreceptor membranes: Immunocytochemical and autoradiographic localization of opsin in smooth vesicles of the inner segment. *J. Cell Biol.* 83:275a (Abstr.).
38. Papermaster, D. S., B. G. Schneider, M. A. Zorn, and J. P. Kraehenbuhl. 1978. Immunocytochemical localization of a large intrinsic membrane protein to the incisures and margins of frog rod outer segment discs. *J. Cell Biol.* 78:415–425.
39. Papermaster, D. S., B. G. Schneider, M. A. Zorn, and J. P. Kraehenbuhl. 1978. Immunocytochemical localization of opsin in outer segments and Golgi zones of frog photoreceptor cells. An electron microscope analysis of cross-linked albumin-embedded retinas. *J. Cell Biol.* 77:196–210.
40. Pfenninger, K. H. 1979. Synaptic membrane differentiation. *In* The Neurosciences: Fourth Study Program. F. O. Schmitt, editor. MIT Press, Cambridge, Mass. 779–795.
41. Raubach, R. A., P. P. Nemes, and E. A. Dratz. 1974. Chemical labeling and freeze-fracture studies on the localization of rhodopsin in the rod outer segment disk membrane. *Exp. Eye Res.* 28:1–12.
42. Röhlich, P. 1975. The sensory cilium of retinal rods is analogous to the transitional zone of motile cilia. *Cell Tissue Res.* 161:421–430.
43. Schacher, S., E. Holtzman, and D. C. Hood. 1976. Synaptic activity of frog retinal photoreceptors a peroxidase uptake study. *J. Cell Biol.* 70:178–192.
44. Sjöstrand, F. S., and M. Kreman. 1978. Molecular structure of outer segment discs in photoreceptor cells. *J. Ultrastruct. Res.* 65:195–226.
45. Sjöstrand, F. S., and M. Kreman. 1979. Freeze-fracture analysis of structure of plasma membrane of photoreceptor cell outer segments. *J. Ultrastruct. Res.* 66:254–275.
46. Wald, G. 1968. Molecular basis of visual excitation. *Science (Wash. D. C.).* 162:230–239.
47. Weibel, E. R., G. Losa, and R. P. Bolender. 1976. Stereological method for estimating relative membrane surface area in freeze-fracture preparations of subcellular fractions. *J. Microsc.* 107:255–266.
48. Yoshikami, S., and W. A. Hagins. 1973. Control of the dark current in vertebrate rods and cones. *In* Biochemistry and Physiology of Visual Pigments. H. Langer, editor. Springer-Verlag, New York. 245–255.
49. Young, R. W. 1967. The renewal of photoreceptor outer segments. *J. Cell Biol.* 33:61–72.
50. Young, R. W., and D. Bok. 1969. Participation of the retinal pigment epithelium in the rod outer segment renewal process. *J. Cell Biol.* 42:392–403.
51. Young, R. W., and B. Droz. 1968. The renewal of protein in retinal rods and cones. *J. Cell Biol.* 39:169–184.